

Lower bounds of altitudes for pulsar γ -ray radiation

K. J. Lee¹, Y. J. Du³, H. G. Wang², G. J. Qiao¹, R. X. Xu¹, J. L. Han³

¹*Astronomy Department, School of Physics, Peking University, Beijing 100871, China (kjlee007@gmail.com)*

²*Center for astrophysics, Guangzhou University, Guangzhou 510400, China*

³*National Astronomical Observatories, Chinese Academy of Sciences, 20A Datun Road, Chaoyang, Beijing 100012, China*

ABSTRACT

Determining radiation location observationally plays a very important role in testing the pulsar radiation models. One-photon pair production in the strong magnetic field, $\gamma - e^+e^-$, is one of the important physical processes in pulsar radiation mechanisms. Photons near pulsar surface with sufficient energy will be absorbed in the magnetosphere and the absorption optical depth for these GeV γ -ray photons is usually large. In this paper, we include the aberrational, rotational and general relativistic effects and calculate the γ -B optical depth for γ -ray photons. Then we use the derived optical depth to determine the radiation altitude lower bounds for photons with given energies. As a case study, we calculate the lower bounds of radiation altitudes of Crab pulsar for photons with energy from 5 GeV to 1 TeV.

Key words: stars — neutron: gamma-rays — theory : methods — data analysis

1 INTRODUCTION

Pulsars are ideal laboratories to test physics rules at extreme environment, yet how the pulsar radiations are generated in pulsar magnetospheres is surely an open question though more observational data are accumulated. Three types of models have been proposed to explain the pulsed γ -ray radiation from pulsars. These models are the polar cap model (Ruderman & Sutherland 1975; Daugherty & Harding 1994), the annular gap model (Qiao et al. 2004, 2007), and the outer gap model (Cheng et al. 1986a,b; Chiang & Romani 1994; Cheng et al. 2000; Zhang et al. 2007). The distinguishing characteristics of these models are the acceleration region for primary particles. The primary acceleration regions locate near the pulsar surface for polar cap models and for the annular gap model¹, but far away in the magnetosphere for outer. The classical outer gap interacts with the annular gap due to the particle out flow out from the annular gap, which behavior similar to the outer gap with boundary currents (Hirotani 2006). The fundamental physics differs in three types of models due to the difference of magnetic field intensity. Observational judgments for the radiation altitudes are therefore very critical to discriminate these radiation models. Early observations indicated a 10 GeV cut-offs in the photon spectrum of γ -ray pulsars (Thompson 2008). Thanks to the improvements of γ -ray observational technologies, recent results both from space-based Fermi Large Area Telescope (FERMI) and from ground-based Cherenkov telescope (MAGIC) confirm such spectra cut-offs and also have observed the high energy tails of the spectra cut-off above 10 GeV (Lopez et al. 2009; Fermi Collaboration 2009a,b). These existing high energy observations shied lights on the altitudes of the pulsar γ -ray radiation regions.

The first order relativistic quantum processes allow interchange of momentum between photons and magnetic field (Erber 1966). The electron-positron pair production becomes no longer forbidden, such that a γ -ray photon with sufficient energy can convert into e^+e^- pairs in strong magnetic field. The cross section for the γ -B process increase with the background magnetic field and photon energy. Since the magnetic field near pulsar surface is usually strong, the γ -B absorption process is capable of developing a spectra cut-off in high energy ends of the pulsar spectra, if γ -ray photons are generated in the vicinity of star surface.

After summarizing the works of Baring & Harding (2001) and Baring et al. (1997), Baring (2004) find an analytical formula to calculate such spectrum cut-off energy as a function of pulsar period, the pulsar surface magnetic field and the radiation location altitude. One can fit the observed γ -ray spectra to a theoretical model to measure the spectra cut-off energy, and then use Baring (2004)’s formula to determine the lower bound for radiation altitude. However in order to measure the

¹ The annular gap model has extended radiation region.

spectrum cut-off energy, one need to include both the absorption effects and the initial photon source function (Baring et al. 1997), which is sensitive to the input radiation model. Naturally one could get different values for the cut-off energy for the same data set by using different theoretical models. So determining the radiation altitude lower bounds by using spectrum cut-off energy is rather model-dependent, because there is no model independent way of defining the value of cut-off energy.

In this paper, we present a model independent method to measure the radiation altitude lower bounds. In fact, one can answer the question about the lower bounds of radiation altitude through a slightly different approach. Instead of using cut-off energy, one can ask what is the lower bound for radiation altitude, such that γ -ray photons with certain energy ε will not be absorbed and can be observed? Here, the term ‘not absorbed photons’ and ‘observable photons’ means those optical-thin photons (Rybicki & Lightman 1986), i.e. photons with optical depth τ less than a prescribed optical depth threshold τ_{th} , where τ_{th} is used to specify the confidence levels for low bounds of the radiation altitude. It turns out that there exists a minimal radius (called *last trapping radius*, r_{tr}), below which the photons are mostly absorbed and convert into e^+e^- pairs in the presence of intense magnetic fields. The existence of such last trapping radius is a consequence of the r^{-3} dependence of dipole magnetic field of pulsar, i.e. we can find a small enough r such that the magnetic field is strong enough to initiate the γ -B absorption for the γ -ray photons with sufficient energy. When pulsed γ -ray emission from a pulsar is detected at a given energy band we can determine the r_{tr} correspondingly. Obviously such r_{tr} is *the lower bound for radiation altitude for photons with certain energy*. Since such lower bounds only involves the optical depth for absorption processes and observing energies, the r_{tr} is a model independent altitude lower bound.

In this paper, we dedicate to investigate the γ -B absorption radiation transfer in the pulsar magnetosphere. The r_{tr} is calculated as a function of the magnetic field configuration of pulsar magnetosphere and the photon energy. Analytical formula are presented in § 2.1. The more precise numerical calculations are made in § 2.2 for different source locations and in § 2.3 for phase resolved absorption. The application to Crab pulsar with the phase resolved lower bounds for radiation altitudes are presented in § 2.4. Conclusions and discussions are given in § 3.

2 γ -B ABSORPTIONS OF HIGH ENERGY PHOTONS IN PULSAR MAGNETOSPHERE

2.1 γ -B absorption—the analytical approach

In this section, we analytically estimate the optical depth and the radius for last trapping surface r_{tr} . The r_{tr} is mathematically defined as the radius, at which the γ -B absorption optical depth is equal to a given threshold optical depth τ_{th} . The probability is less than $e^{-\tau_{\text{th}}}$ for photons to escape from a region with altitude lower than r_{tr} . For examples, when $\tau_{\text{th}} = 1, 10$, the escape probabilities are 37% and 5×10^{-5} respectively (Rybicki & Lightman 1986). Obviously, such probability tells about the confidence of r_{th} as an altitude lower bound,

Here we only consider magnetic field much weaker than 10^{13} Gauss, and the photon energy is much larger than e^+e^- static mass, i.e. much larger than 1 MeV. In this way, we can ignore the photon splitting effect (Baring & Harding 2001). Meanwhile the number of pair states is large enough to allow us ignore the resonance effects due to the finite number of pair states (Daugherty & Harding 1983). The following formula is appropriate to calculate the γ -B absorption coefficient κ (Erber 1966)

$$\kappa = 1.55 \times 10^7 \varepsilon_{[\text{MeV}]}^{-1} K_{1/3}^2 \left(\frac{30.0}{B_{\perp[12]} \varepsilon_{[\text{MeV}]}} \right) \text{cm}^{-1}. \quad (1)$$

The function $K_{1/3}$ is the second type modified Bessel function of order 1/3; $B_{\perp[12]}$ is the magnetic field strength perpendicular to the photon propagating direction in unit of 10^{12} Gauss; and $\varepsilon_{[\text{MeV}]}$ is the energy of photon in unit of MeV.

The photons of 5 GeV to 1 TeV in the pulsar magnetosphere are radiated by ultra-relativistic charged particles, which are approximately beamed along the magnetic field lines. After a photon propagates a length of λ , the angle θ_i between photon direction and local magnetic field becomes $\theta_i \sim \lambda/r_{\text{cur}}$. Here r_{cur} is the curvature radius of magnetic field lines. For dipole magnetic field, we have $r_{\text{cur}} \sim \frac{4}{3} r^{1/2} r_{\text{lc}}^{1/2}$, where r is the altitude of the photon and r_{lc} is the light cylinder radius. Using geometrical unit such that light velocity is 1, we have $r_{\text{lc}} \sim p/(2\pi)$ for the pulsar with period of p . One gets $B_{\perp} \sim \theta_i B = \lambda/r_{\text{cur}} B$, where B is the magnetic field intensity at the altitude. The dipole magnetic field has intensity of $B \sim B_0 R^3/r^3$, with B_0 as the magnetic field intensity at the pulsar surface, and R as the radius of the pulsar. The optical depth $\tau = \int_0^{\infty} \kappa d\lambda$. Because the absorption coefficient κ exponentially dependent on the magnetic field, which is of r^{-3} dependence, the absorption coefficient exponentially decrease as $e^{-\lambda^3/\theta_i}$, when λ is large. The dominant part of the optical depth are thus the integration of λ from 0 to r_s , where r_s is the altitude, at which the photons are generated (see the Appendix for the details). Further more, when $\lambda \leq r_s$, the magnetic field B can be approximately regarded as a constant. Thus the *characteristic absorption length* λ_c is $\lambda_c \simeq r_s$, and the integration for optical depth is then replaced by $\tau \sim \kappa \lambda_c \sim \kappa r_s$, which is later further justified by numerical integration. Thus

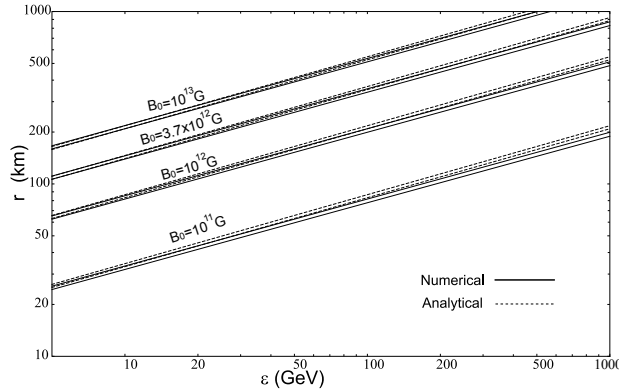


Figure 1. The radius of last trapping surface r_{tr} for different photon energy ε and surface magnetic field. The x-axis is the photon energy, while the star surface magnetic field intensity B_0 are labeled above each curve. For each B_0 there are two groups of curves. Two solid curves are the numerical result from directly solving $\tau(r_{\text{tr}}) = \tau_{\text{th}}$ with $\tau_{\text{th}} = 1, 10$ from the top down. Three dashed curves are analytical solutions from Eq. 4 with $\tau_{\text{th}} = 1, 10$.

$$\tau(r_s) \sim \frac{1.55 \times 10^7 r_{[\text{cm}]}}{\varepsilon_{[\text{MeV}]}} K_{1/3}^2 \left(\frac{2.76 \times 10^6 r_{s,[\text{cm}]}^{5/2} p_{[\text{s}]}^{1/2}}{B_{0,[12]} R_{[\text{cm}]}^3 \varepsilon_{[\text{MeV}]}} \right), \quad (2)$$

where $r_{s,[\text{cm}]}$ is the r_s in unit of cm, $p_{[\text{s}]}$ is the period of a pulsar in unit of second.

By setting $\tau(r_{\text{tr}}) = \tau_{\text{th}}$ and solving for r_{tr} , we get radius of last trapping surface, which should be the lower bounds for the radiation altitude for photons. The numerical solutions to $\tau(r_{\text{tr}}) = \tau_{\text{th}}$ is given in Fig. 1, for different τ_{th} .

We can also get analytical solutions to $\tau(r_{\text{tr}}) = \tau_{\text{th}}$ using asymptotic method. Note that the Bessel function have asymptotic property of $K_{1/3}^2(x) \simeq \pi e^{-2x}/(2x)$. The solution to Eq. 2 can be presented by using the Lambert W function, where function $y = W(x)$ is defined as the solution to equation $ye^y = x$ (Corless et al. 1996). Using the function W and taking $R = 10^6$ cm, the solution to $\tau(r_{\text{tr}}) = \tau_{\text{th}}$ is

$$r_{\text{tr},[\text{cm}]} = 2.6 \times 10^4 B_{0,[12]}^{2/5} \varepsilon_{[\text{MeV}]}^{2/5} p_{[\text{s}]}^{-1/5} W^{2/5} \left(\frac{3.46 \times 10^{20} B_{0,[12]}^{2/3}}{p_{[\text{s}]}^{1/3} \varepsilon_{[\text{MeV}]}^{5/3} \tau_{\text{th}}} \right) \quad (3)$$

which have asymptotic approximation given as

$$r_{\text{tr},[\text{cm}]} \simeq (1.1 \times 10^5 - 1.9 \times 10^3 \ln \tau_{\text{th}}) B_{0,[12]}^{2/5} \varepsilon_{[\text{MeV}]}^{2/5} p_{[\text{s}]}^{-1/5}. \quad (4)$$

This analytical results are plotted together with the numerical results in Fig. 1. The analytical approximation give error of about 20% percent. The effect of τ_{th} is very tiny, due to the logarithmic dependence of τ_{th} as we expect from Eq. 4. We present the results with $\tau_{\text{th}} = 1, 10$. It turns out that the difference between the r_{tr} for $\tau_{\text{th}} = 1$ and for $\tau_{\text{th}} = 100$ is still less than 20%, where the probability for photons escaping region with $\tau_{\text{th}} = 100$ is 10^{-43} times smaller than escaping region with $\tau_{\text{th}} = 1$, or the radiation from region with $\tau_{\text{th}} = 100$ is 10^{-43} times as fainter than radiation from $\tau_{\text{th}} = 1$. This is far beyond dynamical range of instruments and is exactly why we can define the optical thin photons as observable photons and use r_{tr} as the altitude low bound, without going into the details of equipment response.

For the case of Crab pulsar, i.e. $B_{0,[12]} = 3.7$, $p_{[\text{s}]} = 0.033$ (Manchester et al. 2005), we see from Fig. 1 that the radius of the last trapping surface for 5 GeV, 10 GeV, 100 GeV and 1 TeV γ -ray radiation are 100 km, 150 km, 350 km, 850 km respectively.

2.2 γ -B absorption processes with detailed geometry

We have estimated the radius of last trapping surface r_{tr} and taken it as lower bounds of the radiation altitudes for the pulsed pulsar γ -ray radiation. The γ -B process depends on geometries of both photon ray directions and magnetic fields. In this section, we calculate the r_{tr} with detailed geometry.

The γ -B absorption coefficient κ is sensitive to the geometrical parameter θ_i , the angle between the photon propagating direction and the local magnetic field direction. There are five possible geometrical effects that changes the θ_i . These effects are listed as follows. (1). Photons, when generated, are not exactly beamed along local magnetic field lines due to the finite Lorentz factor γ_p of particles. This introduces an increase of θ_i by $\delta\theta_i$, where $\delta\theta_i \sim \gamma_p^{-1} < 10^{-2}$ given $\gamma_p \gg 10^2$ (Rybicki & Lightman 1986). (2). Due to special relativistic effect, the rotational velocity of the pulsar boosts the photons to a new direction, which gives $\delta\theta_i \sim \Omega r \sim r/r_{\text{lc}} \sim 10^{-2}$ for a young pulsar with $p \sim 0.1$ s (Gangadhara 2005), where $\Omega = 2\pi/p$ is the pulsar's rotational angular velocity. The r is choose to be 100 km as order of magnitude estimation from previous section. It should be noted

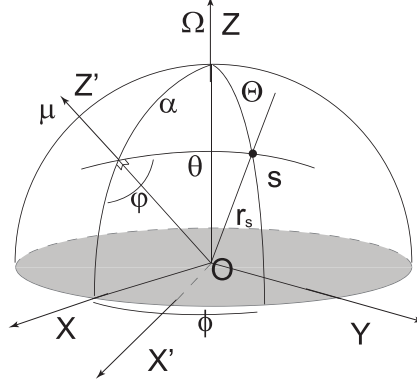


Figure 2. The geometrical configuration for the coordinate systems for calculations. In the laboratory frame $O - XYZ$, the Z axis is aligned with the rotational axis Ω of pulsar. The magnetic frame $O - X'YZ'$ is generated by rotating the $O - XYZ$ coordinate around Y axis by an inclination angle of α , such that the Z' axis is aligned with the dipole magnetic momentum μ . The polar angle and azimuthal angle in laboratory polar coordinate are denote as Θ, Φ , while the polar angle and azimuthal angle in the magnetic polar coordinate are θ, φ . The r_s is the radius for the radiation source.

that we use geometrical unit through out this paper without special mention, i.e. the light speed $c = 1$ and the gravitational constant $G = 1$. (3). The magnetic field is co-rotating with the star, thus after the photon propagates for time of t , the magnetic field has rotated for an angle of Ωt . It gives $\delta\theta_i \sim \Omega t \sim 2\pi r/p \sim 10^{-2}$. (4). Due to the gravitational field of pulsar, the photons propagate along ‘curved’ geodesics rather than ‘straight’ lines. This effect is order of $\delta\theta_i \sim \theta_i m/r \sim 10^{-3}$, as $m \sim 2$ km for 1.4 solar mass pulsar. (5). The pulsar drags the background space co-rotating with it due to gravitomagnetism effects. The space co-rotating angular velocity is Lense-Thirring angular velocity $\omega_{LT} \sim 2m\Omega R^2/r^3$, where R is the pulsar radius. This gives $\delta\theta_i \sim \omega_{LT} t \sim 2m\Omega R^2/r^2 \sim 10^{-7}$. We see that the curved spacetime effect and frame-dragging effects are of higher order geometrical effect compared to other effects, which are coincident with the results of Gonthier & Harding (1994). Therefore, we only consider the aberration effect and the magnetic field rotation effect to correct the geometrical effects to the order of 10^{-2} . This conclusion are valid for short period pulsar ($p \geq 0.1$ s) and higher altitude absorption ($r \geq 100$ km). Thus, we can just use flat space-time geometry (including photon direction and magnetic field direction) to calculate the geometrical parameters (e.g. θ_i).

However, the gravitational effects also play the other two important roles in γ -B processes. (1). The gravitational field makes the photon red shifted, i.e. the energy ε of photons observed by static observer is $\varepsilon = \varepsilon_\infty(1 + \eta)$, where ε_∞ is the photon energy observed by infinite-distant observer and $\eta = m/r$ is the Newtonian gravitational potential. This introduces energy correction by $\varepsilon m/r \sim 10^{-2}\varepsilon$. (2). The dipole magnetic field strength is enhanced due to gravitational effect (Ginzburg & Ozernoy 1964; Anderson & Cohen 1970; Wasserman & Shapiro 1983; Muslimov & Tsygan 1986), which magnetic field intensity correction of order $m/r \sim 10^{-2}$. Both of the two effects are of 10^{-2} order effects. In short, we can use flat space geometry to calculate the geometrical parameters, i.e. θ_i , but the magnetic field and photon energy need the first order gravitational corrections to include effects of 10^{-2} level.

We set up the coordinates as shown in Fig. 2. In the coordinate $O - XYZ$, the Z axis is aligned with the rotational axis Ω of pulsar. This coordinate $O - XYZ$ is called the laboratory frame. Another coordinate, the $O - X'YZ'$, is generated by rotating the $O - XYZ$ coordinate around Y axis by inclination angle α , such that the Z' axis is aligned with the dipole magnetic momentum μ . We call this coordinate the magnetic frame. The two vectors Ω and μ locates in the plane $O - XZ$, which is called $\Omega - \mu$ plane. The polar coordinate associated with $O - XYZ$ and $O - X'YZ'$ are called the laboratory polar coordinate and the magnetic polar coordinate, respectively. The polar angle and azimuthal angle in the laboratory polar coordinate are denoted as Θ, Φ , while the polar angle and azimuthal angle in the magnetic polar coordinate as θ, φ . Here, we use bold type font to label the vector or the matrix; while we use subscript x, y, z and x', y', z' to indicate their component value in the laboratory frame and component value in the magnetic coordinate respectively. The coordinate transformation between two coordinates is given by $\mathbf{a}^i = \mathbf{T}^{ij} \cdot \mathbf{a}'^j$, where \mathbf{a} and \mathbf{a}' are any vectors in laboratory frame and magnetic frame respectively, transformation \mathbf{T}_α^{ij} is the matrix given as

$$\mathbf{T}_\alpha^{ij} = \begin{pmatrix} \cos \alpha & 0 & \sin \alpha \\ 0 & 1 & 0 \\ -\sin \alpha & 0 & \cos \alpha \end{pmatrix} \quad (5)$$

Let’s consider a photon generated at the position ‘S’ in Fig. 2. The initial position of photon \mathbf{r}_s in the magnetic polar coordinate is

$$\begin{pmatrix} r_{s,x'} \\ r_{s,y'} \\ r_{s,z'} \end{pmatrix} = r_s \begin{pmatrix} \sin \theta_s \cos \varphi_s \\ \sin \theta_s \sin \varphi_s \\ \cos \theta_s \end{pmatrix}, \quad (6)$$

where θ_s, φ_s are the polar angle and azimuthal angle for source position 'S' in magnetic frame, and r_s is the radiation altitude. The photon generated at position 'S' propagates along direction \mathbf{n}_B of the local magnetic field for a co-rotating observer. The component value of vector \mathbf{n}_B is easily calculated in magnetic polar coordinates (Swisdak 2006)

$$\begin{pmatrix} n_{B,x'} \\ n_{B,y'} \\ n_{B,z'} \end{pmatrix} = \begin{pmatrix} \frac{3 \cos \theta_s \cos \varphi_s \sin \theta_s}{\sqrt{1+3 \cos^2 \theta_s}} \\ \frac{3 \cos \theta_s \sin \varphi_s \sin \theta_s}{\sqrt{1+3 \cos^2 \theta_s}} \\ \frac{1+3 \cos 2\theta_s}{\sqrt{1+3 \cos^2 \theta_s}} \end{pmatrix},$$

which can be used to calculate the component value of \mathbf{n}_B in laboratory frame by combining it with Eq. 5.

The rotational effect boosts the photon to direction \mathbf{n}_ν , known as the aberration effect. The relation between components of \mathbf{n}_ν and components \mathbf{n}_B is give by Lorentz transformation (Misner et al. 1973)

$$\begin{pmatrix} \chi \\ \chi n_{\nu,x} \\ \chi n_{\nu,y} \\ \chi n_{\nu,z} \end{pmatrix} = \mathcal{L} \cdot \begin{pmatrix} 1 \\ n_{B,x} \\ n_{B,y} \\ n_{B,z} \end{pmatrix},$$

where matrix \mathcal{L} is defined as

$$\mathcal{L} = \begin{pmatrix} \gamma & \gamma v_x & \gamma v_y & 0 \\ \gamma v_x & 1 + (\gamma - 1) \frac{v_x^2}{\beta^2} & (\gamma - 1) \frac{v_x v_y}{\beta^2} & 0 \\ \gamma v_y & (\gamma - 1) \frac{v_x v_y}{\beta^2} & 1 + (\gamma - 1) \frac{v_y^2}{\beta^2} & 0 \\ 0 & 0 & 0 & 1 \end{pmatrix},$$

and γ, β are $\gamma = 1/\sqrt{1 - v_x^2 - v_y^2}$ and $\beta = \sqrt{v_x^2 + v_y^2}$ respectively, χ is the redshift of photon due to aberration effect. The v_x, v_y is the components of co-rotation velocity at the place where photon is generated. The velocity can be calculated by $\mathbf{v} = \boldsymbol{\Omega} \times \mathbf{r}_s$. In the laboratory frame, we have

$$\begin{pmatrix} v_x \\ v_y \\ v_z \end{pmatrix} = r_s \boldsymbol{\Omega} \begin{pmatrix} -\sin \theta_s \sin \varphi_s \\ \cos \theta_s \sin \alpha + \cos \alpha \cos \varphi_s \sin \theta_s \\ 0 \end{pmatrix}$$

After take such aberration effect into account, the equation for component value for \mathbf{n}_ν is

$$\begin{cases} n_{\nu,x} = \frac{3h+f \sin \alpha - r_s \Omega \sin \theta_s \sin \varphi_s [\sqrt{2}b+3dr_s \Omega \sin(2\theta_s) \sin \varphi_s]}{\sqrt{2}gb\chi} \\ n_{\nu,y} = \frac{2bdr_s \Omega + \sqrt{2}[6 \cos \theta_s - dr_s^2 \Omega^2 (3h+f \sin \alpha)] \sin \theta_s \sin \varphi_s}{2gb\chi} \\ n_{\nu,z} = \frac{f \cos \alpha - 3h \tan \alpha}{\sqrt{2}b\chi} \end{cases} \quad (7)$$

where

$$\begin{aligned} g &= \sqrt{1 - r_s^2 \Omega^2 [(\cos \alpha \sin \theta_s \cos \varphi_s + \sin \alpha \cos \theta_s)^2 + \sin^2 \theta_s \sin^2 \varphi_s]}, \\ b &= \sqrt{3 \cos(2\theta_s) + 5}, \\ d &= \cos \alpha \sin \theta \cos \varphi_s + \sin \alpha \cos \theta_s \\ f &= 3 \cos(2\theta_s) + 1, \\ h &= \cos \alpha \sin(2\theta_s) \cos \varphi_s, \\ \chi &= \frac{b + \sqrt{2} r_s \Omega \sin \alpha \sin \theta_s \sin \varphi_s}{gb}. \end{aligned}$$

The position of photon $\mathbf{x}(t)$ is a function of photon propagating time t . With the \mathbf{n}_ν , we can calculate the position of photon by $\mathbf{x}(t) = \mathbf{r}_s + \mathbf{n}_\nu t$. We need to further calculate the magnetic field at each position $\mathbf{x}(t)$ to get the absorption coefficient κ . To do this, we firstly calculate magnetic field in the magnetic polar coordinate and then use coordinate transformation to derive the magnetic field strength at \mathbf{x} .

The magnetic field in the co-rotating magnetic polar coordinate is

$$\mathbf{B}' = \frac{B_0 R^3}{2r^3} \left(1 + \eta \frac{8 + 4 \cos(2\theta)}{5 + 3 \cos(2\theta)} \right) \sqrt{\frac{5 + 3 \cos(2\theta)}{2}} \mathbf{n}_B \quad (8)$$

where r, θ, φ are the radius, polar, and azimuthal angle in the co-rotating magnetic polar coordinate for $\mathbf{x}(t)$, B_0 is the effective surface magnetic field determined from energy losing rate, and $\eta = m/r$ is the Newtonian gravitational potential.

The magnetic field configuration defined in Eq. 8 satisfy two conditions that the magnetic field intensity is concord with results in the Schwarzschild background and the magnetic field direction is concord with the flat background results. Due to the rotation of pulsar, the magnetic field is also ‘rotating’. Then the relation between magnetic field in laboratory frame and the magnetic field in the co-rotation magnetic polar coordinates is $\mathbf{B} = \mathbf{T}_\Omega \cdot \mathbf{T}_\alpha \cdot \mathbf{B}'$, where the transformation \mathbf{T}_Ω is coordinates transformation due to the rotation of the pulsar. The matrix form of \mathbf{T}_Ω is given by

$$\mathbf{T}_\Omega = \begin{pmatrix} \cos \Omega t & -\sin \Omega t & 0 \\ \sin \Omega t & \cos \Omega t & 0 \\ 0 & 0 & 1 \end{pmatrix}.$$

Use this transformation, we can also figure out the relation between the co-rotational magnetic polar coordinates $\{r, \theta, \varphi\}$ and laboratory frame $\{x, y, z\}$, which is given as

$$\begin{pmatrix} x \\ y \\ z \end{pmatrix} = r \mathbf{T}_\Omega \cdot \begin{pmatrix} \cos \theta \sin \alpha + \cos \alpha \cos \varphi \sin \theta \\ \sin \theta \sin \varphi \\ \cos \alpha \cos \theta - \cos \varphi \sin \alpha \sin \theta \end{pmatrix}. \quad (9)$$

Since the photo propagating direction does not change in laboratory frame, the perpendicular magnetic field strength B_\perp is $B_\perp = \sqrt{\mathbf{B} \cdot \mathbf{B} - (\mathbf{B} \cdot \mathbf{n}_\nu)^2}$. When the gravitational redshift of photon is taken into account, we have $\varepsilon = \varepsilon_\infty(1 + \eta)$. In this way, the absorption coefficient κ as a function of t can be calculated using the ε , B_\perp , and Eq. 1. We then integrate κ over t to calculate the optical depth.

We now summarize the steps to calculate the optical depth and the radius of last trapping surface, as follows,

- (i) For a radiation source located at $\{r_s, \theta_s, \varphi_s\}$, we calculate the photon propagating direction \mathbf{n}_ν with Eq. 7;
- (ii) We calculate the photon position after time t using $\mathbf{x}(t) = \mathbf{r}_s + \mathbf{n}_\nu t$;
- (iii) Solve Eq. 9 to calculate the coordinate of photon in magnetic polar coordinate (r, θ, φ) from coordinate of $\mathbf{x}(t)$;
- (iv) Using the photon position (r, θ, φ) to calculate the magnetic field strength according to Eq. 8. Then calculate B_\perp using $B_\perp = \sqrt{\mathbf{B} \cdot \mathbf{B} - (\mathbf{B} \cdot \mathbf{n}_\nu)^2}$;
- (v) Using $\tau(r_s) = \int_0^\infty \kappa(t; r_s) dt$ to calculate the optical depth for the photon coming from position \mathbf{r}_s . The κ is calculated from Eq. 1;
- (vi) Solve $\tau(r_{\text{tr}}) = \tau_{\text{th}}$ respected to r_{tr} to determine the lower bounds for radiation altitude given required τ_{th} ;

There is no analytical solution to $\tau(r_{\text{tr}}) = 1$ respected r_{tr} . We use bi-section method to solve it numerically, while the integration is performed using adaptive integration method to refine a preset logarithmic mesh of t to achieve necessary numerical precision. The results are given in Fig. 3. We also get the results for $\tau_{\text{th}} = 3$ and $\tau_{\text{th}} = 10$, the plots are very similar to Fig. 3 due to the logarithmic dependence of τ_{th} .

The results are different for various inclination angles of pulsars, due to the aberration effect and rotational magnetic field effect. If these two effects would be ignored, the results would be insensitive to inclination angle α . We also see the aberration effects become important for large inclination angles, since the r_s shows larger difference between $\varphi_s = 90^\circ$ (for the leading photon rays) and $\varphi_s = 270^\circ$ (for the trailing photon rays) cases.

2.3 Radiation Geometry and Phase-resolved Lower Bounds for Radiation Altitudes

In this section we determine the radiation location for different longitudinal phase. The details of radiation geometry can be found in Gil et al. (1984); Lyne & Manchester (1988); Lee et al. (2006). We omit the aberration effects here, because it is second order effect for calculating the pulse phase.

Given the pulse profile longitude $\Delta\Phi$ (see Fig. 2 for details) and the view angle ζ , the half angular beam width for the radiation beam θ_μ can be solved by (Gil et al. 1984; Lyne & Manchester 1988)

$$\sin^2\left(\frac{\theta_\mu}{2}\right) = \sin^2\left(\frac{\Delta\phi}{2}\right) \sin \alpha \sin \zeta + \sin^2\left(\frac{\zeta - \alpha}{2}\right), \quad (10)$$

With the θ_μ , the radiation source polar angle θ_s and azimuthal angle φ_s in magnetic polar coordinate can be calculated, where

$$\theta_s = \frac{1}{2} \arccos \left[\frac{\sqrt{\sin^4 \theta_\mu - 10 \sin^2 \theta_\mu + 9} - \sin^2 \theta_\mu}{3} \right], \quad (11)$$

and

$$\varphi_s = \arccos \left[\frac{\cos \alpha \cos \theta_\mu - \cos \zeta}{\sin \alpha \sin \theta_\mu} \right]. \quad (12)$$

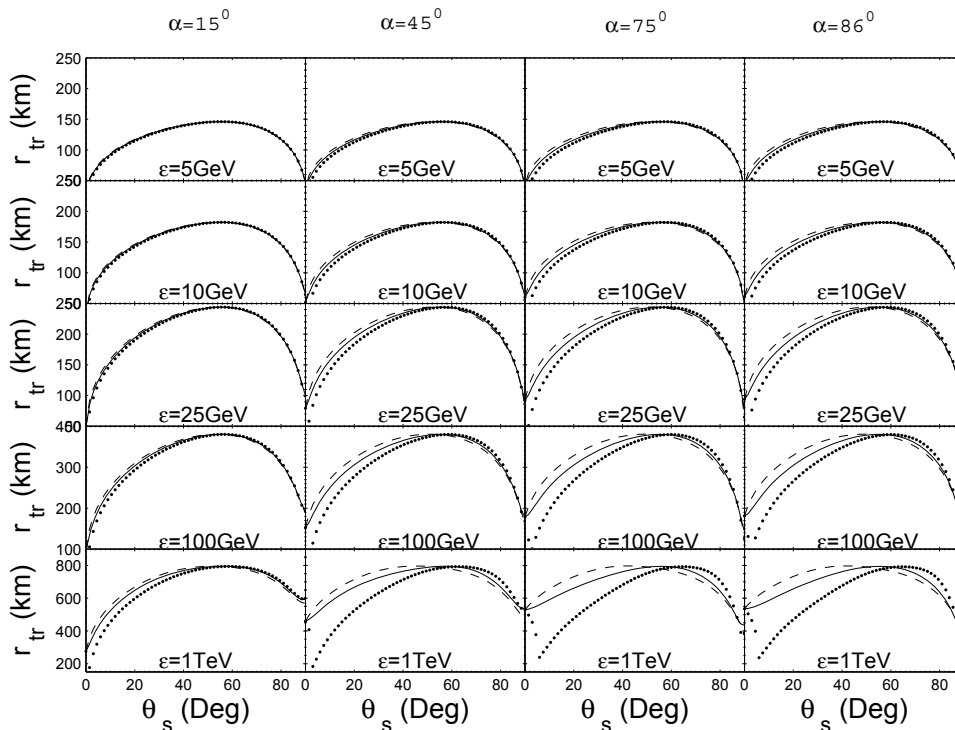


Figure 3. The lower bounds r_{tr} of altitude as functions of radiation source polar angle θ_s . The solid lines, dashed lines and dotted lines correspond to $\varphi_s = 0^\circ$, $\varphi_s = 90^\circ$, and $\varphi_s = 270^\circ$ respectively. The surface magnetic field strength is taken to be $B_0 = 3.7 \times 10^{12}$ Gauss as the Crab pulsar, and the threshold optical depth is set to $\tau_{th} = 1$. The ε is the photon energy used in calculations for each panel, while the inclination angle of pulsar α is labeled on the top of each column. The results for $\tau_{th} = 3$ and $\tau_{th} = 10$ are almost the same as results presented here.

Using Eq. 10, 11, and 12, we can calculate the angular position for radiation source θ_s, φ_s from pulse profile phase $\Delta\Phi$ and view angle ζ . Then we can determine the r_{tr} using the techniques developed in § 2.2. For $\zeta = 60^\circ$ case, the result could be found in Fig. 4.

2.4 Application to Crab pulsar

As a case study, we apply the method for altitude lower bounds to Crab pulsar and obtain the phase resolved altitude lower bounds for 25 GeV γ -ray emission. The view angle of Crab pulsar is taken to be 60° , as measured from X-ray image of Crab nebular (Weisskopf et al. 2000; Wang 2003) and $\alpha \sim 55^\circ - 60^\circ$ by fitting slot gap model or $\alpha \sim 70^\circ$ from fitting outer gap model (Fermi Collaboration 2009b). The surface magnetic field of Crab is taken to be $B_0 = 3.7 \times 10^{12}$ Gauss. The inclination angle for Crab is unknown at this time, thus we calculate the r_{tr} for the four cases, $\alpha = 15^\circ, 45^\circ, 75^\circ, 86^\circ$ ². Assuming the radiation are from single pole, we find that the phase resolved lower bounds are roughly around 250 km for various inclination angles, which is concord with our estimation in §2.1.

For pulsar with inclination angle α and the view angle ζ , we can use Eq. 10, 11, and 12 to calculate the magnetic polar angle θ_s and magnetic azimuthal angle ϕ_s for radiation source, which contribute to pulse profile with longitude $\Delta\Phi$. We use bi-section method to solve $\tau(r_{tr}) = \tau_{th}$ respected to r_{tr} to determine the altitude lower bounds, below which the photon escape probability is less than $e^{-\tau_{th}}$. The numerical results are given in Fig. 4 for $\tau_{th} = 1$ case.

3 DISCUSSIONS AND CONCLUSIONS

In this paper, we derive the basic formalism for calculating the effect of γ -B absorption for γ -ray photons in pulsar magnetosphere. We have considered magnetic field line bending, aberration effect, rotational effects, gravitational red-shift of photons and gravitational effect on magnetic field intensity.

² Rankin (1990) got $\alpha = 86^\circ$

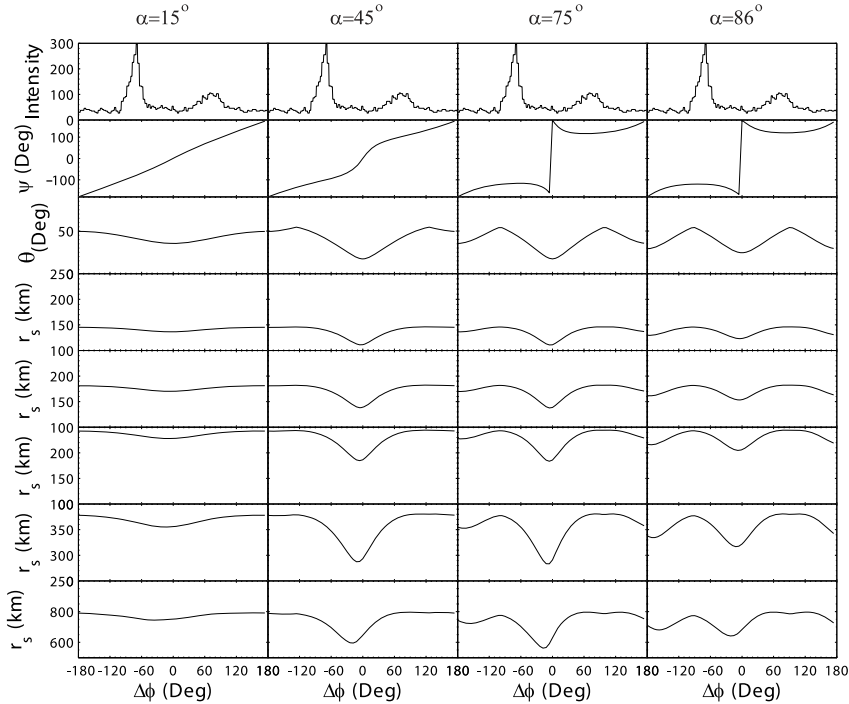


Figure 4. The altitude lower bounds for different pulse longitudes. Each column corresponds to results for different inclination angle α , as labeled on the top. The x-axes are the pulse longitudinal phase. The first row is the pulse profile of Crab observed in above 100 MeV band, the data comes from (Thompson 2001) and is not very different from recent data from FERMI (Fermi Collaboration 2009b); the second and the third row are the azimuthal angle and polar angle of radiation source in magnetic polar coordinate, respectively; the fourth to the eighth row are for the $\tau_{\text{th}} = 1$ radiation altitude lower bounds for $\varepsilon = 5$ GeV, $\varepsilon = 10$ GeV, $\varepsilon = 25$ GeV, $\varepsilon = 100$ GeV, and $\varepsilon = 1$ TeV, respectively. During the calculation, we take $B_0 = 3.7 \times 10^{12}$ Gauss (Manchester et al. 2005), $\zeta = 60^\circ$ (Weisskopf et al. 2000; Wang 2003), and $p = 0.033$ (Manchester et al. 2005) s as Crab pulsar parameters.

In particular, we calculate the altitudes for last trapping surface, at which the photon generated is optical thick ($\tau = 1$) due to γ -B processes both analytically (§ 2.1) and numerically (§2.2). We regard such altitudes as the lower bounds for γ -ray radiation altitude. The analytical estimation and numerical results get good agreement. The numerical calculation suggest slightly higher value (20%) for r_{tr} than analytical calculation, due to approximation for analytical method.

The altitude lower bounds are calculated for different longitudes. For Crab pulsar, the altitude lower bound is about 100 km, 150 km, 250 km, 400 km, and 800 km, for 5 GeV, 10 GeV, 25 GeV, 100 GeV, and 1 TeV γ -ray radiation respectively for various inclination angle. Note that the r_{tr} is larger around $\Delta\phi = 0$. This is a geometrical effect. Because the curvature radius of magnetic field lines are smaller around $\Delta\phi = 0$, the transverse magnetic field intensity B_\perp and the absorption coefficient κ become smaller. Although beyond the measured cut-off energy, 10 GeV pulsed emission is confirmed, 150 km radiation altitude lower bounds could falsify the classical polar cap model for pulsar's γ -ray radiation (Daugherty & Harding 1994). However it can not discriminate present pulsar γ -ray radiation model including slop gap model (Harding et al. 2008), outer gap model (Cheng et al. 1986a,a; Chiang & Romani 1994; Cheng et al. 2000) and inner annular gap model (Qiao et al. 2004). We can neither exclude possibility for a high altitude model producing a low energy cut-off as indicated in (Harding et al. 2008), since such cut-off may be due to intrinsic physical conditions.

We see that the lower bounds r_{tr} is not sensitive to τ_{th} , mainly due to the logarithmic dependence of τ_{th} , as we have already seen in Eq. 4. Thus the difference between r_{tr} for $\tau_{\text{th}} = 1$ and $\tau_{\text{th}} = 10$ is less than 10%.

The magnetic field components of higher order magnetic momentum decrease much faster than that of the dipole magnetic momentum. Therefore for the emission from high altitudes ($r/R \sim 10^{-2}$), we can thus ignore the higher order magnetic momentum than dipole, although the higher order magnetic momentum are important near the star surface (Ruderman & Sutherland 1975).

Our results give different value compared to Baring (2004). The main reason is the difference of treating photon characteristic absorption length. A brief comparison is given in the appendix of this paper. It is shown that Baring (2004)'s result under-estimates the characteristic absorption length, such that it needs stronger magnetic field to achieve absorption, which under estimate the r_{tr} .

The cut-off is not a good radiation location indicator. Firstly, it is not only sensitive to data quality but also sensitive to the data reduction processes, i.e. how the cut-off is fitted (Lopez et al. 2009). Secondly, there are still pulsed emission photons coming from the cut-off tails. Thirdly, one needs to model the initial photon population to make reasonable result for cut-off energy. Thus we only use the observation fact that photons of energy ε are detected, then we discuss where is the lowest possible position (i.e. r_{tr}), above which the photons can just propagate freely without strong absorption by pulsar magnetic field. Such r_{tr} is well defined. Future measurement of cut-off energy will not change the conclusion here, as far as 10 GeV pulse emission of the Crab pulsar has been confirmed, the radiation altitude of 150 km we calculated for the lower bounds holds.

Seven pulsars were detected in γ -ray bands previously (Thompson 2008), and more than 40 γ -ray pulsars are just found recently e.g. (Fermi Collaboration 2009a; Pellizzoni et al. 2009). FERMI (Harding & Fermi LAT Collaboration 2009) and AGILE are now seeking for more γ -ray pulsars. If young γ -ray pulsars with stronger magnetic field are observed at higher energy (e.g. 1 TeV) in the future, there would be a great challenge to the slop gap model and annular gap model. Future γ -ray pulsar searching and the follow up observations using ground based Cherenkov telescope ares expected to test present γ -ray radiation models for pulsars.

We are grateful to C.K. Chou for reading the paper. We are also grateful to L. Guillemot and A. Jessner for reading the paper and giving valuable comments improving the paper. This work was supported by NSFC (10833003, 10778611, 10821061) and the National Basic Research Program of China (Grant 2009CB824800).

REFERENCES

- Anderson, J. L., & Cohen, J. M. 1970, *ApSS*, 9, 146
 Baring, M. G. 2004, *Advances in Space Research*, 33, 552
 Baring, M. G., & Harding, A. K. 2001, *ApJ*, 547, 929
 Baring, M. G., Harding, A. K., Gonthier, P. L., 1997, *ApJ*, 476, 246
 Cheng, K. S., Ho, C., & Ruderman, M. 1986a, *ApJ*, 300, 500
 —. 1986b, *ApJ*, 300, 522
 Cheng, K. S., Ruderman, M., & Zhang, L. 2000, *ApJ*, 537, 964
 Chiang, J., & Romani, R. W. 1994, *ApJ*, 436, 754
 Corless, R. M., Gonnet, G. H., Hare, D. E. G., Jeffrey, D. J., & Knuth, D. E. 1996, *Advances in Computational Mathematics*, 5, 329
 Daugherty, J. K., & Harding, A. K. 1983, *ApJ*, 273, 761
 —. 1994, *ApJ*, 429, 325
 Erber, T. 1966, *Reviews of Modern Physics*, 38, 626
 Fermi Collaboration, 2009, astro-ph:0910.1608v1, submit to *ApJ*
 Fermi Collaboration, 2009, astro-ph:0911.2412, submit to *ApJ*
 Gangadhara, R. T. 2005, *ApJ*, 628, 923
 Gil, J., Gronkowski, P., & Rudnicki, W. 1984, *A&A*, 132, 312
 Ginzburg, V. L., & Ozernoy, L. M. 1964, *JETP*, 47, 1030
 Gonthier, P. L., & Harding, A. K. 1994, *ApJ*, 425, 767
 Harding, A. K., & Fermi LAT Collaboration. 2009, in *Bulletin of the American Astronomical Society*, Vol. 41, Bulletin of the American Astronomical Society, 480
 Harding, A. K., Stern, J. V., Dyks, J., & Frackowiak, M. 2008, *ApJ*, 680, 1378
 Hirotani, K. 2006, *ApJ*, 652, 1475
 Lee, K. J., Qiao, G. J., Wang, H. G., & Xu, R. X. 2006, *Advances in Space Research*, 37, 1988
 Lopez, M., Otte, N., Rissi, M., Schweizer, T., Shayduk, M., Klepser, S., for the MAGIC Collaboration, 2009, astro-ph:09070832
 Lyne, A. G., & Manchester, R. N. 1988, *MNRAS*, 234, 477
 Manchester, R. N., Hobbs, G. B., Teoh, A., & Hobbs, M. 2005, *Astron. J*, 129
 Misner, C. W., Thorne, K. S., & Wheeler, J. A. 1973, *Gravitation* (San Francisco: W.H. Freeman and Co., 1973)
 Muslimov, A. G., & Tsygan, A. I. 1986, *Soviet Astronomy*, 30, 567
 Pellizzoni et al. 2009, *ApJL*, 695, L115
 Qiao, G. J., Lee, K. J., Wang, H. G., Xu, R. X., & Han, J. L. 2004, *ApJL*, 606, L49
 Qiao, G. J., Lee, K. J., Zhang, B., Wang, H. G., Xu, R. X. 2007, *CJAA*, 7, 496
 Rankin, J. M. 1990, *ApJ*, 352, 247
 Ruderman, M. A., & Sutherland, P. G. 1975, *ApJ*, 196, 51
 Rybicki, G. B., & Lightman, A. P. 1986, *Radiative Processes in Astrophysics* (Wiley-VCH)
 Swisdak, M. 2006, astro-ph:0606044v1

The Magic Collaboration. 2008, *Science*, 322, 1221

Thompson, D. J. 2001, in *American Institute of Physics Conference Series*, Vol. 558, American Institute of Physics Conference Series, ed. F. A. Aharonian & H. J. Völk, 103

Thompson, D. J. 2008, *Reports on Progress in Physics*, 71, 116901

Wang, H. G. 2003, PhD thesis, Peking University, China

Wasserman, I., & Shapiro, S. L. 1983, *ApJ*, 265, 1036

Weisskopf et al. 2000, *ApJL*, 536, L81

Zhang, L., Fang, J., & Cheng, S. B. 2007, *ApJ*, 666, 1165

APPENDIX A: COMPARISON BETWEEN BARING'S RESULTS AND RESULTS IN THIS PAPER

This paper answers a different question compared with Baring (2004). We are discussing the altitude lower bound for observed photons with specific energy, while Baring (2004) discussed the spectra cut-off for collective photons. Nevertheless it is interesting to see the difference of the results in Baring (2004)'s and here. It turns out that we will get Baring (2004)'s results, if the characteristic absorption length λ_c is taken to be constant, which corresponds to the case where radiation region is near the star surface.

Following Eq. 19 of Ruderman and Sutherland (1975), the $\gamma - B$ absorption criteria is $\varepsilon_{\text{MeV}} B_{\perp} / B_{\text{cr}} > \chi$, where Such criteria is also adopted by Baring (2004). Due to the curvature of magnetic field, we have $B_{\perp} \sim B \sin \theta_i \sim B \lambda_c / r_{\text{cur}} \sim B_0 \frac{R_0^3}{r_s^3} \frac{\lambda_c}{r_{\text{cur}}}$. So the absorption criteria is

$$\varepsilon_{\text{MeV}} \frac{B_0}{B_{\text{cr}}} \left(\frac{R_0}{r_s} \right)^3 \frac{\lambda_c}{r_{\text{cur}}} > \chi \quad (\text{A1})$$

Substitute $r_{\text{cur}} = \frac{4}{3} \left(\frac{pr_s c}{2\pi} \right)^{1/2}$, we have

$$\varepsilon_{\text{Max, [MeV]}} < \chi \frac{B_{\text{cr}}}{B_0} \left(\frac{r_s}{R_0} \right)^3 \frac{(pr_s c / 2\pi)^{1/2}}{\lambda_c}, \quad (\text{A2})$$

which is just

$$\varepsilon_{\text{Max, [GeV]}} = \left[10^{-2} \chi \sqrt{c/2\pi} \frac{R_0^{1/2}}{\lambda_c} \right] \sqrt{p} \left(\frac{r_s}{R_0} \right)^{1/2} \frac{0.1 B_{\text{cr}}}{B_0} \left(\frac{r_s}{R_0} \right)^3, \quad (\text{A3})$$

If we take $\lambda_c / \chi = 17$, we just get Baring (2004)'s results

$$\varepsilon \simeq 0.4 \sqrt{p} \left(\frac{r_s}{R_0} \right)^{1/2} \max \left\{ 1, 0.1 \frac{B_{\text{cr}}}{B_0} \left(\frac{r_s}{R_0} \right)^3 \right\} \text{ GeV}. \quad (\text{A4})$$

If we take $\lambda_c = r_s$, we go back to Eq. 4. The reason for making such choice is illustrated in Fig. A1. There are two comparative factors dominant the tendency of absorption coefficient κ . Firstly, the impact angle θ_i between photon direction and local magnetic field grows with λ then saturated to a limited value due to pure geometrical relation. Secondly, magnetic field intensity decrease approximately following $(r_s + \lambda)^{-3}$ due to dipole field configuration. Thus the perpendicular magnetic field strength $B_{\perp} \sim B \theta_i$ follows relation $\lambda / (r_s + \lambda)^{-3}$. The absorption coefficient κ depends on B_{\perp} exponentially. So θ_i , B and κ follow the dashed, dot-dashed and solid curve in Fig. A1 respectively. Clearly the effective absorption length takes value of r . Precisely speaking, there must be some numerical fact η (due to integration and geometry), where $\eta \simeq 1$, such that $\lambda_c = \eta r_s$. In practical, this η can be regarded as been accounted and put into the threshold optical depth τ_{th} . Due to the dependence of r_{tr} on τ_{th} is logarithmic (see Eq. 4), such correction of η is not important. This is why the analytical estimation is concord with the numerical calculation developed in section 2.2.

Clearly at high altitude, the characteristic absorption length λ_c is no long a constant and must be treated as a function of radiation altitude. Because of the implicit assumption of a constant characteristic absorption length, Baring (2004) results under-estimate the characteristic absorption length λ_c so does the optical depth. This leads to smaller r_{tr} as we have seen for high altitude radiation. We have used $\lambda_c \sim r_s$ as argued in this paper to derive Eq. 4, which is later checked by our numerical results. For low energy photons (a few GeV), our results agree with Baring & Harding (2001) because the characteristic absorption length is about the size of star.

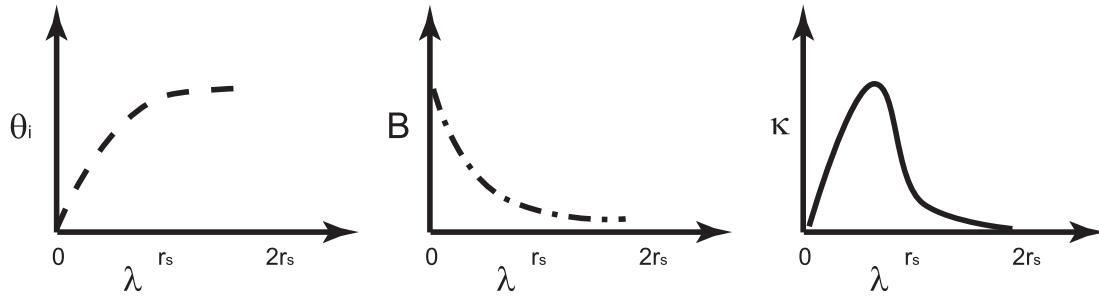


Figure A1. The illustration for the relation between γ -B impact angle θ_i , magnetic field intensity B , absorption coefficient κ and photon propagating length λ . θ_i , B and κ follow the dashed, dot-dashed and solid curve respectively when λ grows from 0 to large values.